ELSEVIER

Materials Science and Engineering A 422 (2006) 29–40

MATERIALS SCIENCE & ENGINEERING A

www.elsevier.com/locate/msea

Reflection electron energy loss spectroscopy of nanometric oxide layers and of their interfaces with a substrate

Fabien Paumier [a,b,*], Valérie Fouquet [a], Marie-Jo Guittet [a], Martine Gautier-Soyer [a], Roger H. French [c,d], Guolong Tan [c], Yet Ming Chiang [e], Ming Tang [e], Ana Ramos [a,e], Sung-Yoon Chung [e]

[a] *Service de Physique de Chimie des Surfaces et des Interfaces, DSM/DRECAM/SPCSI, CEA Saclay, 91191 Gif sur Yvette Cedex, France*
[b] *Laboratoire de Métallurgie Physique—UMR 6630 CNRS, Department of Materials Sciences, University of Poitiers, France*
[c] *Department of Materials Science and Engineering, University of Pennsylvania, 3231 Walnut Street, Philadelphia, PA 19104, USA*
[d] *DuPont Central Research, E356-384 Experimental Station, Wilmington, DE 19880, USA*
[e] *Department of Materials Science and Engineering, Massachusetts Institute of Technology, Cambridge, MA, USA*

Received in revised form 17 November 2005

Abstract

The aim of the present work was to evaluate the ability of reflection electron energy loss spectroscopy (REELS) as a non-destructive method to obtain depth profiles of dielectric constants, in a complementary way to transmission electron energy loss spectroscopy (TEELS). Two prototypical samples were used: a $SrTiO_3$ single crystal and a 2 nm thick SiO_2 layer on a Si single crystal. The single scattering cross-sections were decomposed into bulk, surface and interface contributions, with Drude–Lorentz parameters of the dielectric function fitted on available optical or TEELS data. We show that the evolution of the shape of the REELS single scattering cross-section with primary energy is qualitatively well reproduced by our model. In the case of the 2 nm SiO_2 layer on Si, introducing the Si/SiO_2 interface energy loss function contribution proved necessary to account for the interface plasmon peak observed, in very good agreement with reported TEELS measurements. REELS is well suited to studying dielectric properties of interfaces between a substrate and a nanometric layer.

Keywords: Electron energy loss spectroscopy; Silicon oxide; Plasmons; Strontium titanate; Thin films

1. Introduction

In the last 10 years reflection electron energy loss spectroscopy (REELS) has raised a renewed interest, particularly on the theoretical side, where a great effort has been devoted to calculate REELS spectra [1–5]. As a result, the number of published experimental studies has increased as well [6–12]. The motivation for this effort has been twofold.

First is the search to further develop quantitative surface analysis. An improved description of the inelastically scattered electrons has been continuously seeked for, so as to achieve a correct removing of the background under the Auger or photoelectron lines [13–17]. The energy losses undergone by the primary electrons in REELS are indeed of the same nature as those undergone by the Auger or photo-electrons. Moreover, REELS has been shown to be a well-suited method to determine the inelastic mean free path, which is an essential parameter in quantitative surface analysis (Auger, X-ray photoemission spectroscopy) [2,7,18,19].

Another strong motivation is in the field of materials science. From a REELS spectrum it is in principle possible to derive the optical dielectric constant $\varepsilon(\omega)$ following the well-established approach used in transmission electron energy loss spectroscopy (TEELS) [20]. Within the range of validity of the dielectric theory, the probability that an electron travelling in a medium of dielectric function $\varepsilon(q,\omega)$ undergoing an inelastic scattering process characterized by a momentum transfer q and an energy loss $\hbar\omega$ is determined by the energy loss function (ELF) $\mathrm{Im}[-1/\varepsilon(q,\omega)]$. Within the optical limit ($q=0$) both the transverse and longitudinal dielectric function $\varepsilon(0,\omega)$ coincide so that the TEELS spectrum will approach the optical energy loss function $\mathrm{Im}[-1/\varepsilon(0,\omega)]$, once multiple scattering is removed.

* Corresponding author. Tel.: +33 549496747; fax: +33 549496692.
E-mail address: fabien.paumier@univ-poitiers.fr (F. Paumier).

0921-5093/$ – see front matter © 2006 Elsevier B.V. All rights reserved.
doi:10.1016/j.msea.2006.01.005

Kramers Kronig analysis then allows the determination of the real part of $(-1/\varepsilon(\omega))$, provided that the refraction index is known. This makes it possible to easily obtain the dielectric function $\varepsilon(\omega)$ from TEELS measurements in the low loss region [20]. In REELS however, low energy incident electrons (100–1000 eV) are used, and the dipolar approximation is no longer valid. The q-dependence of the dielectric function must therefore be taken into account. Moreover, surface excitations cannot be neglected, and different theoretical approaches have been developed to describe these bulk/surface contributions properly.

Several models have been developed to quantitatively calculate the experimental REELS spectra [1–5], based on the pioneering work of Ritchie [21]. To the best of our knowledge, these theoretical models are restricted to homogeneous samples. The comparison between experiment and theory is usually performed with simple elements, like pure metals and silicon. Some recent papers however have been published in which REELS is quantitatively used on more complex compounds like oxides, nitrides or carbides, using Tougaard's model [6,7,19]. The REELS spectra are taken for a set of different primary energies and the experimental inelastic single scattering cross-sections are compared to the ones calculated with a test dielectric constant, the parameters of which are adjusted so that a good matching with experiment is obtained with the same dielectric constant at every primary energy.

What makes REELS particularly interesting is its surface sensitivity. The probed depth is related to the inelastic mean free path, and according to the currently used TPP formula [22], the inelastic mean free path (IMFP) of electrons with a primary energy in the range 100–1000 eV is between 0.5 and 2 nm. Very recently it has been claimed, on the basis of REELS measurements, that these calculated IMFP were even overestimated for ultra thin films in the nanometer range [7]. The drawback of this surface sensitivity is that the proper modelling of REELS spectra is much more tricky than in the case of TEELS. However, due to its probing depth in the nanometer range, REELS is well-suited to characterize nanometric oxide layers, relevant to spin electronic applications (e.g. tunnel barriers in magnetic tunnel junctions) or to future development of microelectronics (e.g. high k gate dielectrics thin films on Si).

As the probing depth can be varied by changing the primary energy of the electron beam, one can expect in essence to obtain non-destructive REELS depths profiles, where the evolution of the REELS spectrum translates to the in-depth evolution of the dielectric constant. Such an information is most valuable when studying interfaces between a nanometric film on a substrate. It was our strong motivation in the NANOAM (Nanometer scale induced structure between amorphous layers and crystalline materials) project to evaluate the ability of REELS to depth profiling, by analogy with the TEELS approach where dielectric functions profiles can be obtained across an interface [23]. In REELS, increasing the primary energy leads to several competing effects. An increased bulk contribution at higher energy means that by tuning the primary energy one can get a contribution of the film/substrate interface, and characteristic loss features of this interface will show up. In addition, the increased bulk contribution of the film itself will contribute and modify the overall shape of the REELS spectrum as well. Therefore, it is of great importance to understand how the REELS spectrum evolves with primary energy even in an in-depth homogenous sample. From a very practical point of view, when dealing with technological samples, a small residual carbon contamination is not always possible to remove without altering the sample. This may also affect the REELS spectrum, with a more pronounced effect at the lowest primary energies. In some cases this might even be a hindrance to the proper analysis of REELS spectra.

The present paper is focused on the variation of surface/bulk contribution in the REELS spectrum as a function of primary energy. We have chosen two prototypical samples: a $SrTiO_3$ (0 0 1) single crystal, and a 2 nm thick SiO_2 layer on a silicon (0 0 1) wafer. The first sample was chosen because the dielectric properties of $SrTiO_3$ are well known, TEELS measurements on $SrTiO_3$ being available for comparison [24]. Moreover, this study could provide reference data for a future REELS study of $SrTiO_3$ nanometric films relevant to applications in metal–insulator–metal (MIM) capacitors. The second sample enables us to evaluate the ability of REELS as a non-destructive method to get depth profiles, in comparison to reported TEELS studies of SiO_2/Si interfaces [25,26].

In the present work, the REELS spectra have been recorded for a set of different primary energies. From each of them a single scattering cross-section was obtained by removing the multiple scattering contribution using Tougaard's algorithm [27]. Our goal here was not to derive a dielectric constant profile from the REELS spectra, but, as a preliminary step, to qualitatively understand the differences in shape arising when the primary energy of electrons changes. So we have used a simplified model where the experimental single scattering cross-sections are described by a linear combination of bulk $\mathrm{Im}[-1/\varepsilon]$ and surface $\mathrm{Im}[-1/(1+\varepsilon)]$ electron energy loss functions [28–31]. The dielectric function was written as an expansion of Drude–Lorentz oscillators, the parameters of which were fitted from optical or TEELS data. Although it is well known that a linear contribution of bulk and surface energy loss functions cannot provide a quantitative description of REELS spectra [19,32], our simplified model accounts fairly well for the overall evolution of the shape of the scattering cross-sections with primary energy. Moreover, it presents the asset of being very well suited for describing a sample consisting of different layers, containing several interfaces. The full accurate calculations of REELS are usually, to the best of our knowledge, restricted to homogeneous samples [1–5]. In the case of the Si/SiO_2 sample, valuable information on the interface dielectric properties could be gained, and compared to reported TEELS studies of the same kind of systems [25,26].

2. Experimental and results

The REELS experiments were performed in a VG Instruments, Inc., ESCALAB Mark II, fitted with an electron gun LEG 200, with a base pressure around 5×10^{-11} mbar. The primary energy could be varied between 100 and 1000 eV. The hemispherical analyser was fitted with a five-channeltron multidetection system. With a pass energy of 20 eV, the full width at half maximum height (FWHM) of the elastic peak varied between

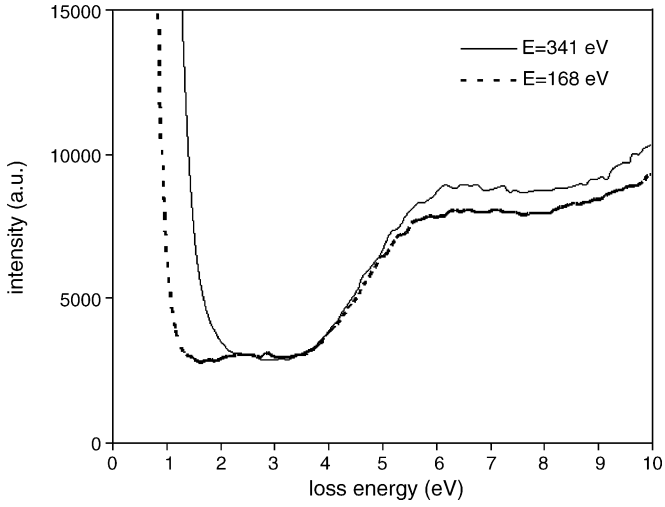

Fig. 1. Low loss energy part of the REELS spectra of $SrTiO_3$ ($E_p = 341$ and 168 eV).

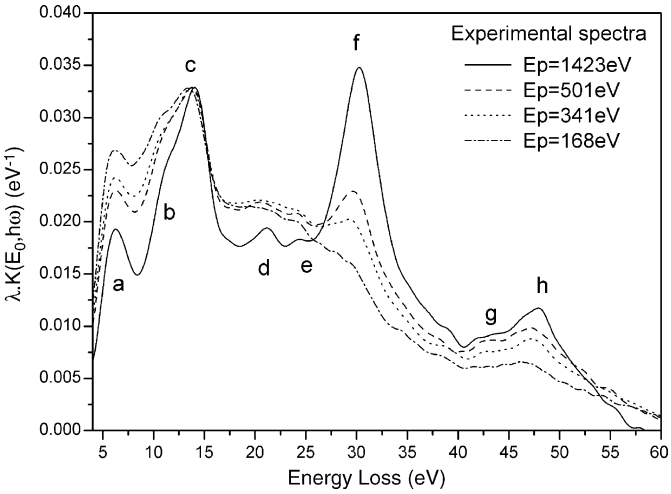

Fig. 2. Single scattering cross-section derived from the experimental REELS spectra of $SrTiO_3$ ($E_p = 168$, 341, 501 and 1423 eV).

0.8 eV for the lowest primary energy up to 1.2 eV at 1000 eV. The current was kept very low, only a few nanoamperes, so as to minimize surface charging under the electron beam on insulating samples. The electron beam was at 35° from the surface normal, while the analyzer axis was at 15° from the surface normal.

From the experimental REELS spectra, an experimental single-scattering cross-section $\lambda K(\hbar\omega)$ was obtained using the QUASES REELS software [33], followed by a deconvolution of the instrumental broadening (taken as the FWHM of the elastic peak, fitted by a Gaussian function). In the following the energy loss is written ΔE or $\hbar\omega$.

The $SrTiO_3$ (0 0 1) single crystal was cleaned ultrasonically in ethanol before loading into ultra-high vacuum. No other attempt was made to further clean the sample, so as to avoid modifying the surface. As a result, a small carbon contamination was still present on the surface, as observed by XPS. From the Sr/C intensity ratio, it was estimated to less than one monolayer. REELS spectra were taken at four different primary energies (168, 341, 501 and 1423 eV). A 3.7 eV band gap was clearly observed in the spectra with the lowest primary energies, for which the FWHM of the elastic peak is lower (Fig. 1). This is in good agreement with the optical value [34]. For the lowest primary energy, a small hump-like structure is observed at an energy loss of 2.5 eV. This structure is likely to be due to a surface defect, as already observed by Henrich and Cox [35]. In this earlier work, a 2.2 eV loss structure appeared after ion bombardment of the surface, likely attributed to oxygen vacancies. Fig. 2 shows the experimental single-scattering cross-section $\lambda K(\hbar\omega)$ obtained from the REELS spectra.

A Si (0 0 1) wafer was cleaned in HF and organic solvents to remove all the native oxide on the surface. The cleaned wafer was then placed in a glass tube under vacuum (2×10^{-5} mbar), with a small amount of CeO_2 powder placed in an edge of the sample. This powder served as an additional oxygen source for the thermal oxidation of the silicon substrate. The sample was annealed for 48 h at 700 °C. As a result, a 2 nm oxide layer was formed on the silicon substrate, as verified by XPS from the ratio of the Si 2p photoelectron lines components (pure Si and Si–O). As for the $SrTiO_3$ sample, the carbon contamination was less than one monolayer. Fig. 3a and b displays the experimental single scattering cross-sections $\lambda K(\hbar\omega)$ obtained at different primary energies ranging from 176 to 1024 eV.

3. Modelling the bulk/surface contribution from the REELS spectra

Assuming that all inelastic multiple scattering has been removed from the experimental REELS spectrum, the obtained single-scattering cross-section contains information on both surface and bulk single-scattering.

As stated in the introduction, recent works have clearly shown that an accurate determination of the dielectric function cannot be achieved by assuming that the experimental single scattering cross-section is a linear combination of bulk and surface electron energy loss functions. Moreover, models have been proposed to fully calculate an effective single scattering cross-section which takes into account the q-dependence of the dielectric function [1,4,5]. These models give a good description of the relative intensities of the peaks in the REELS spectra and in particular of the evolution of the intensity and width of the surface and bulk plasmon peaks versus the primary energy. However, these models are restricted to homogeneous samples, and are difficult to apply to samples with a layer/substrate interface. In addition, when dealing with complex materials such as oxide materials, the q-dependence of the dielectric function is usually unknown. In the present work, our purpose was to settle a very simple model as a help to understand the variations of the experimental scattering cross-sections with primary energy, applicable to a homogeneous sample as well as to a layer/substrate interface. Thus, we have chosen to describe the experimental scattering cross-sections as a linear combination of the bulk and surface electron energy loss functions, expecting this crude model to account for the trends experimentally observed when varying the primary energy.

We first consider a homogeneous sample with a single solid/vacuum interface and then we extend the model to a

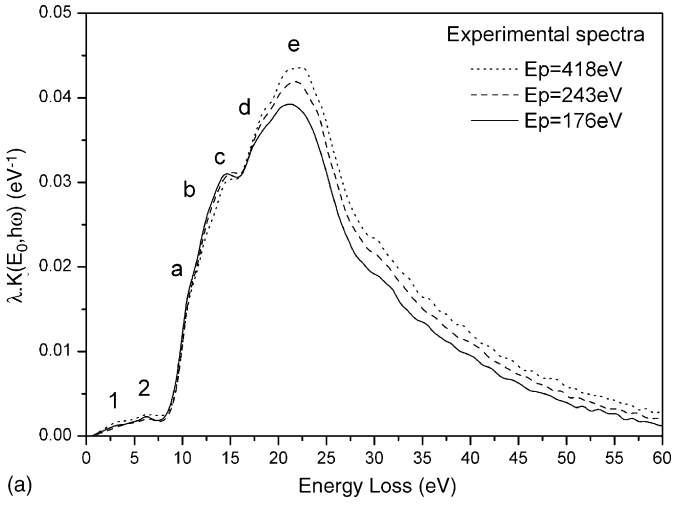

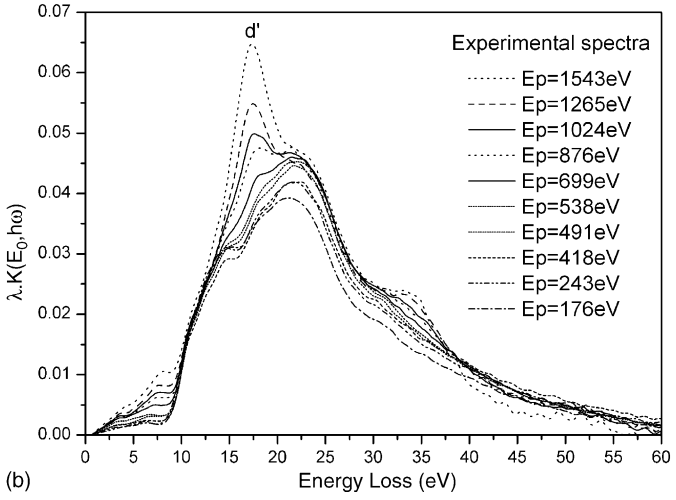

Fig. 3. Single scattering cross-section derived from the experimental REELS spectra of the 2 m SiO_2 layer on Si substrate: (a) $E_p = 176, 243, 418$ eV; (b) from $E_p = 176$ to 1543 eV.

substrate covered by a nanometric layer, with a substrate/layer interface and a layer/vacuum interface.

3.1. Homogeneous sample with a solid/vacuum interface

In order to decompose this single scattering cross-section into its bulk and surface contributions, it was written as a linear combination of bulk $\mathrm{Im}[-1/\varepsilon(\omega)]$ and surface $\mathrm{Im}[-1/(1+\varepsilon(\omega))]$ energy loss functions (Eq. (1)). The weighting coefficients A and B include attenuation terms assuming that the electrons near the surface (at a depth $z = d_1$ below the surface $z = 0$) excite mainly surface losses, while those coming from a depth larger than d_1 excite both bulk and surface (Eqs. (2) and (3)).

$$\lambda K(E_0, \hbar\omega) = A(\lambda(E_\mathrm{p}), \varphi, \phi)\,\mathrm{Im}\left[\frac{-1}{\varepsilon(\omega)}\right] + B(\lambda(E_\mathrm{p}), \varphi, \phi)\,\mathrm{Im}\left[\frac{-1}{1+\varepsilon(\omega)}\right] \quad (1)$$

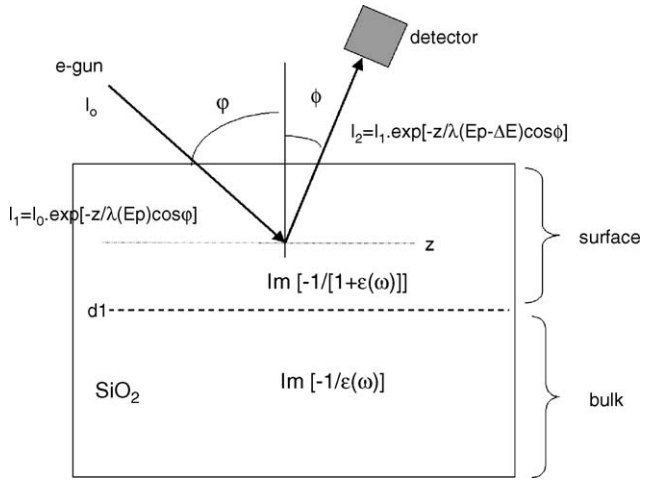

Fig. 4. Geometry of the REELS experiment, in the case of a homogeneous sample with a solid/vacuum interface. The d_1 distance is used in Eqs. (2) and (3).

with

$$\varepsilon(\omega) = \varepsilon_1(\omega) + i\varepsilon_2(\omega)$$

$$\mathrm{Im}\left[\frac{-1}{\varepsilon(\omega)}\right] = \frac{\varepsilon_2}{\varepsilon_1^2 + \varepsilon_2^2}$$

$$\mathrm{Im}\left[\frac{-1}{\varepsilon(\omega)+1}\right] = \frac{\varepsilon_2}{(\varepsilon_1+1)^2 + \varepsilon_2^2}$$

and

$$A(\lambda(E_\mathrm{p}), \varphi, \phi, Z) = A(E_\mathrm{p}) \int_{d_1}^{\infty} \mathrm{d}z \exp\left(\frac{-z}{\lambda(E_\mathrm{p})\cos\varphi}\right) \times \exp\left(\frac{-z}{\lambda(E_\mathrm{p} - \Delta E)\cos\phi}\right) \quad (2)$$

$$B(\lambda(E_\mathrm{p}), \varphi, \phi, Z) = A(E_\mathrm{p}) \int_{0}^{d_1} \mathrm{d}z \exp\left(\frac{-z}{\lambda(E_\mathrm{p})\cos\varphi}\right) \times \exp\left(\frac{-z}{\lambda(E_\mathrm{p} - \Delta E)\cos\phi}\right) \quad (3)$$

λ is the inelastic mean free path (IMFP) calculated using the TPP formula [22], fitted by a straight line in the energy range under consideration. The geometry of the experiment is depicted in Fig. 4, where φ and ϕ are the incidence and detection angles measured from the surface normal. The $A(E_\mathrm{p})$ coefficient depends on the primary energy and takes into account the experimental conditions. Here only one elastic scattering event is considered, multiple elastic scattering events should be taken into account by the $A(E_\mathrm{p})$ coefficient.

The dielectric function $\varepsilon(\omega)$ is written as an expansion of Drude–Lorentz oscillators (Eq. (4)), with no dependence on the momentum transfer q [36].

$$\varepsilon(\omega) = 1 - \frac{f_0\omega_\mathrm{p}^2}{\omega^2 - i\gamma_0\omega} - \sum_{j=1}^{n} \frac{f_j\omega_\mathrm{p}^2}{\omega^2 - \omega_j^2 - i\gamma_j\omega} \quad (4)$$

ω_p is the bulk plasmon frequency $\omega_p = \sqrt{n\,e^2/\varepsilon_0 m^*}$; m^* is the free electron mass, n is the total charge density (in the valence band); γ_0 is the inverse of the relaxation time of the electrons in the valence band ($\gamma_0 = 1/\tau_0$); f_0 is an oscillator strength that describes the free electron contribution to $\varepsilon(\omega)$.

The interband transitions denoted by the subscript j are characterized by the parameters ω_j, f_j and $1/\gamma_j$, which are, respectively, the frequency, the oscillator strength and the lifetime. $f_j = n_j/n$ is the density of electrons bound with resonance frequency ω_j.

The model dielectric function satisfies the following sum rule:

$$\int_0^\infty \omega\varepsilon_2(0,\omega)\,\mathrm{d}\omega = \frac{\pi}{2}\omega_p^2 \Leftrightarrow \sum_{j=1}^{n} f_j = 1$$

For Si, SiO_2, the set of parameters of the dielectric function was fitted to the optical dielectric constant [37]. For $SrTiO_3$, the $\mathrm{Im}[-1/\varepsilon(\omega)]$ energy loss function was calculated using Eq. (4) and the set of parameters was fitted to the TEELS energy loss function [24]. As no q-dependence was taken into account in the dielectric function, it proved necessary to allow the γ_j parameters to further vary when fitting the REELS experimental single scattering cross-sections, all the other parameters remaining unchanged. However, once fitted, the same set of parameters for the dielectric function was used for all the primary energies (see Section 4), and the $A(E_p)$, d_1-values were determined for every primary energy.

3.2. Extended model: Si substrate covered by a SiO_2 nanometric layer

Now we consider a Si substrate covered by a SiO_2 nanometric layer. Two interfaces have to be taken into account: the Si/SiO_2 interface and the SiO_2/vacuum interface. Compared with Eq. (1), new terms have been added to describe the SiO_2/Si interface and the silicon contributions (Eq. (5)). The first term is a simplified expression of the differential probability of scattering at a single interface introduced by Raether [38] and the second is the classical bulk silicon ELF. As for the description of the surface and bulk energy loss function, each component is weighted by an attenuation coefficient (Eqs. (6)–(10)) which depend on the primary energy through the IMFP term. Four thicknesses d_j ($j = 1, 2, 3, 4$) are introduced to locate each component and to describe the ratio between the different ELF (Fig. 5). The interface energy loss function $\mathrm{Im}[-2/(\varepsilon^{SiO_2}(\omega) + \varepsilon^{Si}(\omega))]$ appears twice in Eq. (5), with coefficients C and D, in order to account for the different IMFP values in SiO_2 and in Si (Eqs. (8) and (9)). If we assume constant thicknesses for d_1, d_2, d_3 and d_4, only two free parameters will be used for a given primary energy: $A^{SiO_2}(E_p)$ and $A^{Si}(E_p)$.

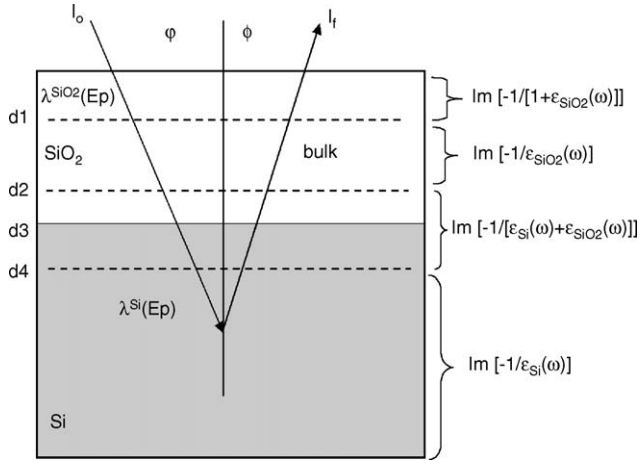

Fig. 5. Si substrate (in grey) covered by a SiO_2 layer (in white). The d_1–d_4 distances are used in Eqs. (6)–(10).

$$\begin{aligned}\lambda K(E_p,\hbar\omega) = {} & A(\lambda^{SiO_2}(E_p),\varphi,\phi)\,\mathrm{Im}\left[\frac{-1}{\varepsilon^{SiO_2}(\omega)}\right] \\ & + B(\lambda^{SiO_2}(E_p),\varphi,\phi)\,\mathrm{Im}\left[\frac{-1}{1+\varepsilon^{SiO_2}(\omega)}\right] \\ & + C(\lambda^{SiO_2}(E_p),\varphi,\phi)\,\mathrm{Im}\left[\frac{-2}{\varepsilon^{SiO_2}(\omega)+\varepsilon^{Si}(\omega)}\right] \\ & + D(\lambda^{Si}(E_p),\varphi,\phi)\,\mathrm{Im}\left[\frac{-2}{\varepsilon^{SiO_2}(\omega)+\varepsilon^{Si}(\omega)}\right] \\ & + E(\lambda^{Si}(E_p),\varphi,\phi)\,\mathrm{Im}\left[\frac{-1}{\varepsilon^{Si}(\omega)}\right] \end{aligned} \quad (5)$$

where

$$A(\lambda(E_p),\varphi,\phi,Z) = A^{SiO_2}(E_p)\int_{d_1}^{d_2}\mathrm{d}z\exp\left(\frac{-z}{\lambda^{SiO_2}(E_p)\cos\varphi}\right) \times \exp\left(\frac{-z}{\lambda^{SiO_2}(E_p-\Delta E)\cos\phi}\right) \quad (6)$$

$$B(\lambda(E_p),\varphi,\phi,Z) = A^{SiO_2}(E_p)\int_{d_2}^{d_1}\mathrm{d}z\exp\left(\frac{-z}{\lambda^{SiO_2}(E_p)\cos\varphi}\right) \times \exp\left(\frac{-z}{\lambda^{SiO_2}(E_p-\Delta E)\cos\phi}\right) \quad (7)$$

$$C(\lambda(E_p),\varphi,\phi,Z) = A^{SiO_2}(E_p)\int_{d_2}^{d_3}\mathrm{d}z\exp\left(\frac{-z}{\lambda^{SiO_2}(E_p)\cos\varphi}\right) \times \exp\left(\frac{-z}{\lambda^{SiO_2}(E_p-\Delta E)\cos\phi}\right) \quad (8)$$

$$D(\lambda(E_p),\varphi,\phi,Z) = A^{Si}(E_p)\int_{d_3}^{d_4}\mathrm{d}z\exp\left(\frac{-z}{\lambda^{Si}(E_p)\cos\varphi}\right) \times \exp\left(\frac{-z}{\lambda^{Si}(E_p-\Delta E)\cos\phi}\right) \quad (9)$$

$$E(\lambda(E_p),\varphi,\phi,Z) = A^{Si}(E_p)\int_{d_4}^{\infty}\mathrm{d}z\exp\left(\frac{-z}{\lambda^{Si}(E_p)\cos\varphi}\right) \times \exp\left(\frac{-z}{\lambda^{Si}(E_p-\Delta E)\cos\phi}\right) \quad (10)$$

4. Discussion

4.1. $SrTiO_3$

In the experimental $\lambda K(\hbar\omega)$ from Fig. 2, the main loss features show up at 6.2 eV (a), 10.4 eV (b), 14 eV (c), 22 eV (d), 24.3 eV (e), 30 eV (f), 42.4 eV (g) and 47.9 eV (h), as measured on the spectrum taken at 1423 eV primary energy. These loss energies are very close to those measured by TEELS [24,39], although the relative intensities are different because of the surface contribution in REELS. The origin of these loss structures has been extensively discussed in Ref. [24]. Structures (a–c) are due to interband transitions from O 2p to Ti 3d and Sr 4d states; structures (d and e) from Sr 4p to Ti 3d and Sr 4d; the loss structure at 30 eV (f) is mainly due to the bulk plasmon of $SrTiO_3$ [40]; the loss structures (g and h) are due to transitions originating from the Sr 4s and Ti 3p deeper electronic levels.

When the primary energy decreases, there is an increase in the intensity of the low loss energy part of the spectrum, while at larger loss energies the intensity decreases, especially in the bulk plasmon peak region.

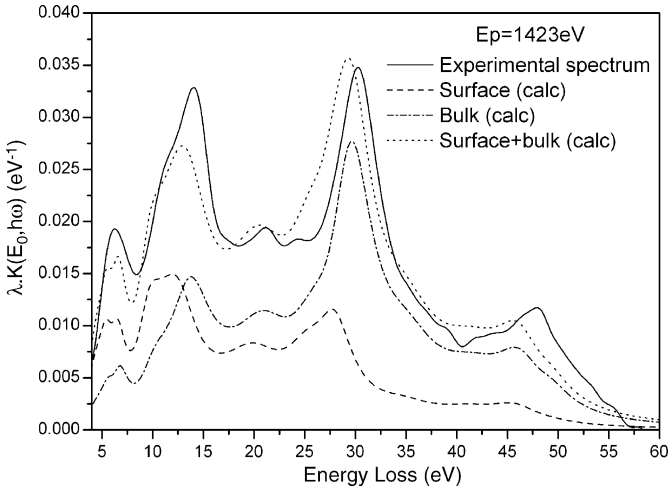

Fig. 6. Decomposition of the experimental single scattering cross-section at $E_p = 1423$ eV into bulk and surface contributions, by using the parameters ($\omega_j f_j \gamma_{j\,\mathrm{TEELS}}$) from Table 1 for the dielectric function of $SrTiO_3$.

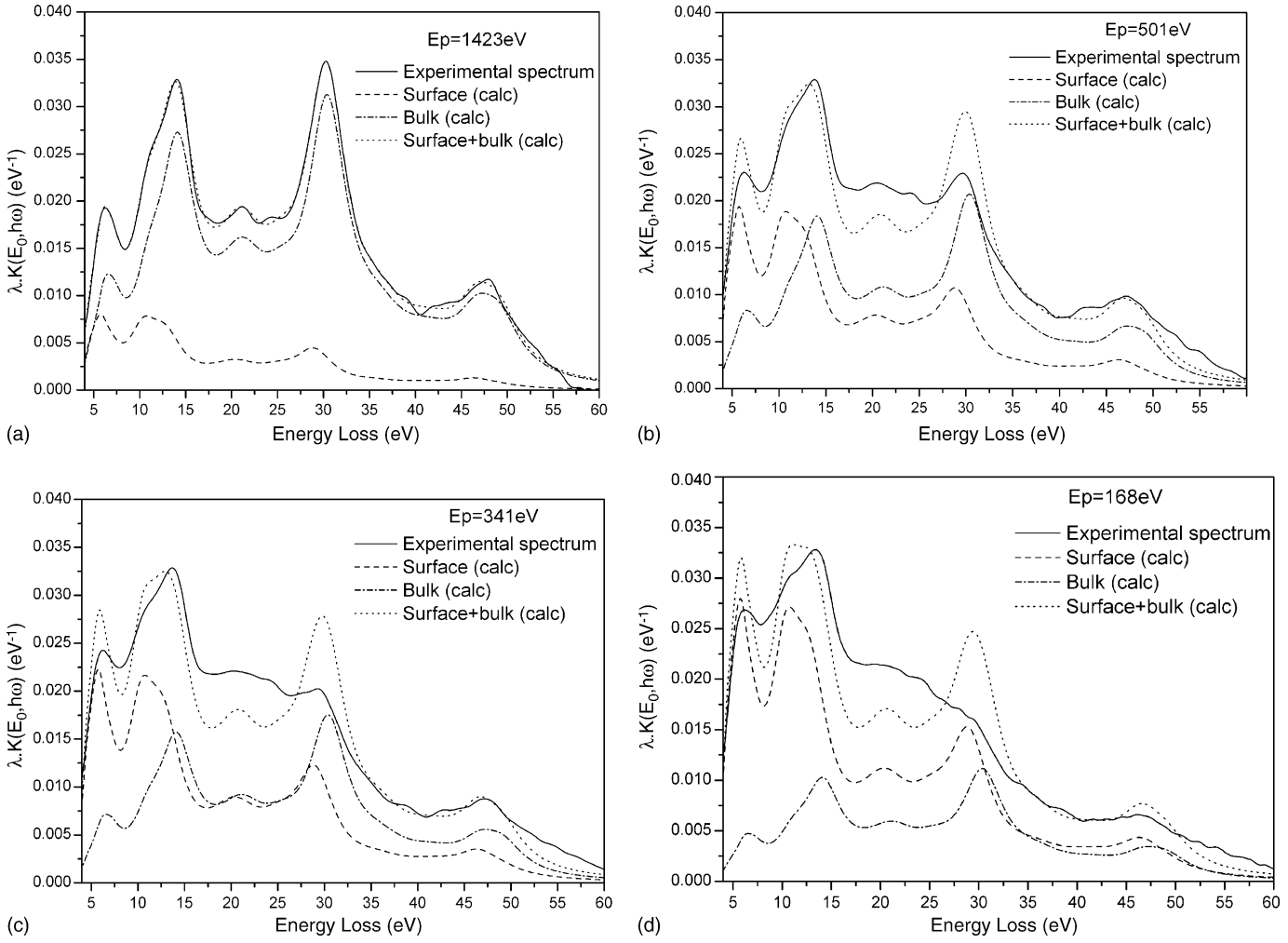

Fig. 7. Decomposition of the experimental single scattering cross-section into bulk and surface contributions, by using the parameters ($\omega_j f_j \gamma_{j\,\mathrm{REELS}}$) from Table 1 for the dielectric function of $SrTiO_3$: (a) $E_p = 1423$ eV; (b) $E_p = 501$ eV; (c) $E_p = 341$ eV; (d) $E_p = 168$ eV.

Table 1
Drude–Lorentz coefficients for the dielectric constant of $SrTiO_3$ (Eq. (4))

j	$\hbar\omega_j$ (eV)	f_j (eV^2)	$\hbar\gamma_j$ (eV)	
			TEELS	REELS
0	25.42	0.189	0.001	0.001
1	4.6	0.045	3.21	3.53
2	6.05	0.007	1.507	2.12
3	8.19	0.099	2.388	3.67
4	11.27	0.059	5.41	5.14
5	18.92	0.14	8.10	7.24
6	24.58	0.07	5.81	5.64
7	27.23	0.141	3.77	5.07
8	34.75	0.031	7.21	6.84
9	41.36	0.063	9.19	8.87
10	45.6	0.086	5.8	5.67
11	48.75	0.07	4.134	5.11

Table 2
A- and d_1-values obtained when decomposing the experimental REELS scattering cross-sections of $SrTiO_3$ at different E_p into bulk and surface contributions according to Eqs. (1)–(3)

E_p	A	d_1 (nm)
TEELS	0.046	0
1423	0.003	0.66
501	0.009	0.69
341	0.012	0.64
168	0.019	0.61

The first line (TEELS) gives the values obtained by using the $\gamma_{j\,\mathrm{TEELS}}$ coefficients at $E_p = 1423$ eV. The other lines are obtained by using the $\gamma_{j\,\mathrm{REELS}}$ values from Table 1.

To describe more quantitatively this evolution of the REELS spectra with the primary energy, we have used the model depicted in Section 3.1. The dielectric function was written as in Eq. (4) and the parameters were fitted from the valence-TEELS data assuming that it was a pure $\mathrm{Im}(-1/\varepsilon)$ function with no q-dependence [24]. The parameters of the dielectric function of $SrTiO_3$ are given in Table 1. Using Eqs. (1)–(3), the parameters $A(E_p)$ and d_1 were first fitted for $E_p = 1423$ eV (Fig. 6). $A(E_p)$, d_1 and the parameters $(\hbar\omega_j, f_j)$ of $\varepsilon(\omega)$ were then kept constant, while the γ_j coefficients which were allowed to change with respect to their initial values $\gamma_{j\,\mathrm{TEELS}}$ in order to fit the experimental $\lambda K(\hbar\omega)$ at $E_p = 1423$ eV. This variation of the γ_j coefficients was necessary to account in some way for the q-dependence, as the initial parameters for $\varepsilon(\omega)$ were fitted from data in the dipolar approximation ($q = 0$). The broadening of the loss peaks, due to the q-dependence in REELS was reproduced by fitting the γ_j coefficients ($\gamma_{j\,\mathrm{REELS}}$) on the experimental $\lambda K(\hbar\omega)$ for $E_p = 1423$ eV (Table 1). The final result of the fit is shown in Fig. 7a, with the bulk and surface contributions. Not only are the widths of the peaks changed when adjusting the γ_j parameters, but their relative intensities as well. This is why the surface and bulk contributions derived from the fit in Fig. 7a do not look exactly like the surface and bulk energy loss contributions of Fig. 6. For the fits of the experimental $\lambda K(\hbar\omega)$ at the other primary energies, all the parameters $(\hbar\omega_j, f_j, \gamma_{j\,\mathrm{REELS}})$ of $\varepsilon(\omega)$ were kept the same as for $E_p = 1423$ eV (Table 1). Only the parameters $A(E_p)$ and d_1 were allowed to vary when fitting the experimental $\lambda K(\hbar\omega)$. The d_1-value did not vary very much and stayed within the range of 0.6–0.7 nm (Table 2), in good agreement with the expected value of approximately 0.5 nm for the thickness of the layer where surface excitations occur [2]. Fig. 7a–d shows separately the experimental $\lambda K(\hbar\omega)$ inelastic cross-sections, along with the fitted ones, as the sum of surface and bulk contributions. Fig. 8 shows the comparison of the fitted single scattering cross-sections at different primary energies. The increase of the intensity in the low loss energy region, along with the decrease of the intensity at larger loss energies, especially in the plasmon peak region, is well reproduced, particularly in the low loss energy region (loss energy < 15 eV). However, the intensity decrease at loss energies larger than 25 eV is much more pronounced in the experimental $\lambda K(\hbar\omega)$ (Fig. 2) than in the simulated ones (Fig. 8). This discrepancy is due to the presence of a carbon monolayer on the surface. Actually the REELS data were analyzed in the frame of an homogeneous sample, but the thin carbon monolayer on top of the sample induced characteristic loss structures, especially a broad one around 20 eV corresponding to the excitation of a plasmon in the carbon layer [8,12,30]. This broad structure is responsible for the significant difference between experiment and simulation in the energy region around 20 eV. Such an effect has already been observed in TEELS, where the carbon contamination occurred in the microscope as a function of irradiation time under the electron beam [24,39].

The comparison experiment/data simulation within our very simple model of an homogenous solid shows that the evolution of the REELS spectrum with the primary energy was not only due to a different weight in the surface/volume contributions, but also to an increased contribution of the carbon contamination layer when the primary energy decreases. It is well known that REELS is very sensitive to surface contamination, and this is a limitation to the study of real samples, which cannot be prepared in situ, and for which it is not always possible to completely remove the carbon. While qualitative REELS might be performed on technological samples, slightly carbon contaminated, quantitative

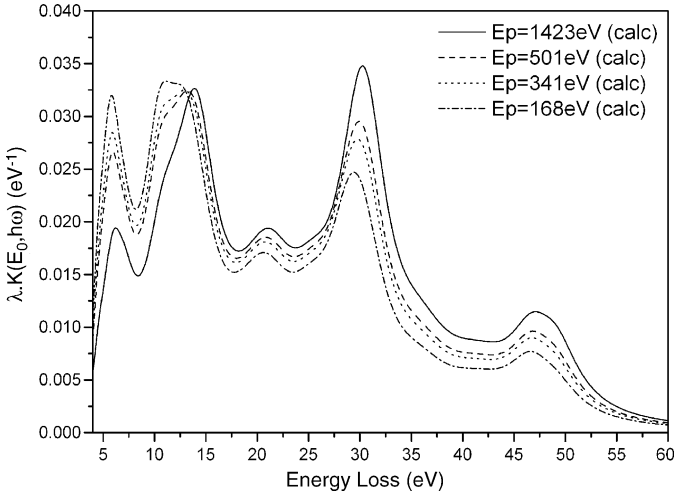

Fig. 8. Comparison of the fitted single scattering cross-sections at $E_p = 1423$, 501, 341 and 168 eV. These fitted single scattering cross-sections are labelled "surface + bulk (calc)" in Fig. 7a–d.

Table 3
Main loss structures showing up in the experimental REELS scattering cross-sections of the SiO_2/Si sample at different primary energies (Figs. 3a and 10)

Energy (eV)	1	2	IPP	*A*	*b*	*c*	*d*	*e*
176	2.98	6.25		10.55	12.44	14.2	17.35	≈21.2 (broad structure)
243	3.77	6.23		10.53	12.6	14.34	17.78	
418	2.98	6.2		10.5	12.3	14.43	17.7	
490	3.14	6.6		10.6	12.26	14.45	17.92	
538	2.98	6.43		10.8	12.63	14.42	18.11	
	1′	2′					*d*′	
698	3.21	5.2	7	10.6	12.51	14.42	17.7	≈21.2 (broad structure)
876	3.28	5.49	7.24	10.7	12.48	14.46	17.49	
1024	3.34	5.61	7.32	10.7	12.43	14.37	17.21	
1265	3.56	5.29	7.35	10.5	12.13	14.4	17.11	
1543	3.7		7.67	10.9	13.3		17.1	

REELS should be rather restricted to atomically clean samples, as the superimposed carbon induced loss structure around 20 eV modifies the relative intensities in this energy region. However, it seems that this affects mainly the loss spectrum above 25 eV. The low energy loss region is affected to a much lesser extent. It thus remains quite possible to measure a reasonable band gap, with a flat band gap region, as shown in Fig. 1.

4.2. *Si/SiO₂ interface*

We first qualitatively describe the experimental REELS single scattering cross-sections of Fig. 3a. At the lowest primary energies (176, 243 and 418 eV) the IMFP are approximately 0.95, 1.14 and 1.55 nm, respectively, which are less than the thickness of SiO_2. The SiO_2 layer is primarily probed, and the single scattering cross-sections look very much the same as the one of SiO_2 [41]. The main structures show up at 10.5 eV (a), 12.5 eV (b), 14.4 eV (c), 17.8 eV (d) and a broad structure is centered around 21.2 eV (e) (Table 3). Two small peaks around 3 eV (1) and 6 eV (2) are observed in the band gap region. These loss energies were determined by using the second derivative of the single scattering cross-section. These peaks are commonly attributed as the fingerprint of a small amount of SiO on the top of the SiO_2 film [17]. Peak a is an exciton, while peaks b, c and d are related to interband transitions. The broad structure around 21.2 eV is due to the bulk plasmon excitation in SiO_2. When the primary energy increases from 176 to 418 eV, the shape changes slightly, with an increase in the intensity of the broad structure (e). To understand this change of shape in this energy range, we have used as a first step the simple model described in Section 3.1 with only a solid/vacuum interface.

The parameters ($\hbar\omega_j$,f_j,$\gamma_{j\,\mathrm{optical}}$) of the dielectric function of SiO_2 were obtained by fitting experimental optical data [37] (Table 4). First the two free parameters $A(E_p)$ and d_1 were adjusted to the experimental curve for $E_p = 176$ eV (Fig. 9a). In Fig. 9a, the surface and bulk contributions are proportional to the optical bulk and surface energy loss functions. The maxima of the bulk energy loss function are at 10.6 eV (a), 12.5 eV (b), 14.75 eV (c), 18.5 eV (d) and 23.4 eV (e), while the maxima of the calculated surface energy loss function are at 10.6 eV (a), 12 eV (b), 14.25 eV (c), 18 eV (d) and 21.38 eV (e). The maxima of the bulk and surface energy loss functions are very close to each other and to the energies of the loss structures as well. In a second step, still for $E_p = 176$ eV (Fig. 9b), only the γ_j parameters were allowed to vary, all other parameters held constant, leading to a new set of γ_j parameters: $\gamma_{j\,\mathrm{REELS}}$ (Table 4). As in Section 4.1, changing the γ_j parameters changed the width and relative intensities of the structures, so that the bulk and surface contributions in Fig. 9b do not look exactly the same as the bulk and surface contributions in Fig. 9a. For $E_p = 243$ and 418 eV, the ($\hbar\omega_j$,f_j,$\gamma_{j\,\mathrm{REELS}}$) parameters from Table 4 were used and $A(E_p)$ and d_1 were adjusted. The results are given in Table 5. As in the case of $SrTiO_3$, the d_1 thickness remained in the 0.6–0.7 nm range. Fig. 9c and d shows the fits obtained for $E_p = 243$ and 418 eV.

Table 4
Drude–Lorentz coefficients for the dielectric function of SiO_2 (Eq. (4))

j	$\hbar\omega_j$ (eV)	f_j (eV^2)	$\hbar\gamma_j$ (eV)	
			Optical	REELS
0	19.49	1.7E−05	0.001	0.001
1	16.7	0.19	3.50	7.4
2	13.61	0.128	2.26	5.52
3	11.63	0.084	1.21	2.56
4	10.36	0.041	0.44	1.24
5	21.24	0.219	6.5	9.72
6	34.99	0.325	17.7	21.9

The differences in the experimental single scattering cross-sections observed in Fig. 3a come from the increased weight

Table 5
A- and d_1-values obtained when decomposing the experimental REELS scattering cross-sections of the SiO_2/Si sample at different E_p into bulk and surface contributions according to Eqs. (1)–(3)

E_p	*A*	d_1 (nm)
Optical	0.025	0.68
176	0.025	0.68
243	0.020	0.59
418	0.013	0.62

The first line (optical) gives the values obtained by using the $\gamma_{j\,\mathrm{optical}}$ coefficients at $E_p = 176$ eV. The other lines are obtained by using the $\gamma_{j\,\mathrm{REELS}}$ values from Table 4.

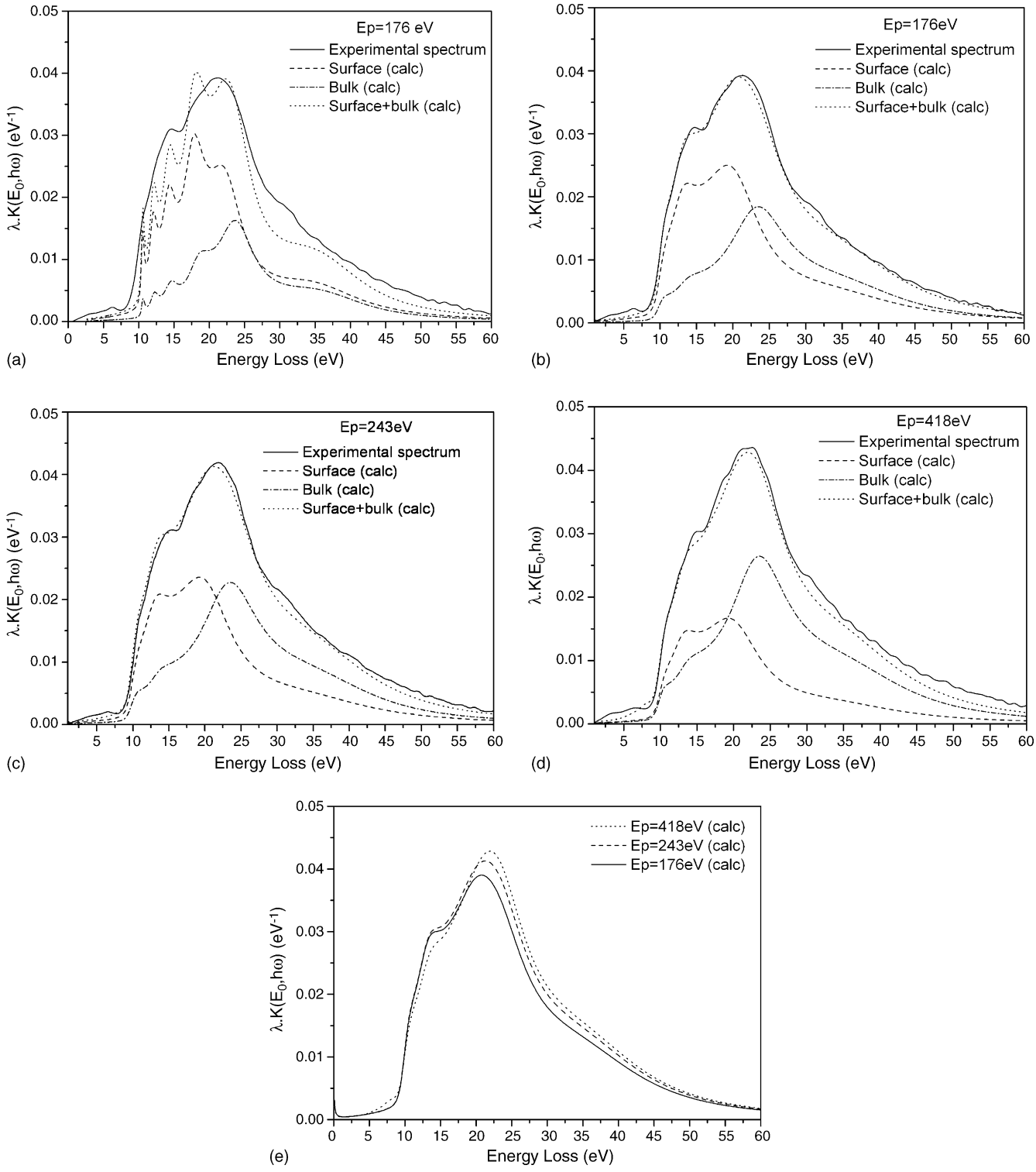

Fig. 9. Decomposition of the experimental single scattering cross-section into bulk and surface contributions by using the parameters (ω_j,f_j,$\gamma_{j\,\mathrm{optical}}$) from Table 4 for the dielectric function of SiO_2: (a) $E_p = 176$ eV and by using the parameters (ω_j,f_j,$\gamma_{j\,\mathrm{REELS}}$) from Table 4 for the dielectric function of SiO_2, (b) $E_p = 176$ eV, (c) $E_p = 243$ eV, (d) $E_p = 418$ eV. (e) Comparison of the fitted single scattering cross-sections at $E_p = 176$, 243 and 418 eV. These fitted single scattering cross-sections are labelled "surface + bulk (calc)" in panels (b–d).

of the bulk contribution when the energy increases, as demonstrated by the comparison between the calculated scattering cross-sections (Fig. 9e). The peaks in the band gap are not reproduced here because no SiO optical data have been introduced in the model.

When the primary energy increases, so does the probing depth. At about 699 eV, the intensity of the structure at 17 eV increases steadily (Fig. 3b). This structure corresponds to the bulk plasmon of silicon (d'). An additional structure at 34 eV develops as well, due to a double plasmon excitation, showing

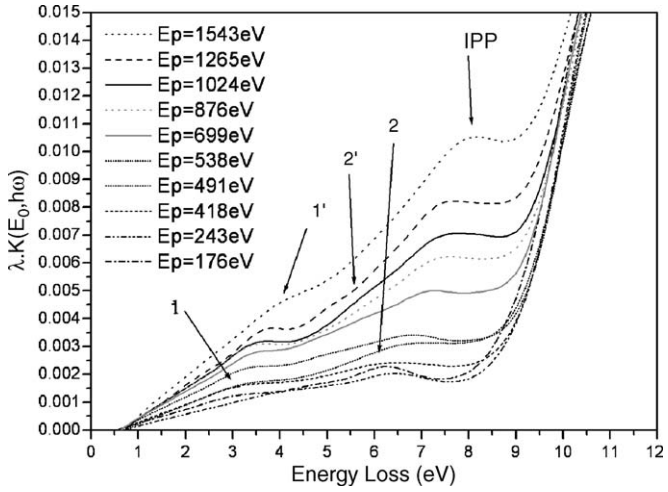

Fig. 10. Enlargement of the low loss energy part of Fig. 3b.

that the multiple scattering removal is not perfect in the present case. As the inelastic mean free path at 699 eV is of the order of 2 nm, which is the thickness of the SiO_2 film, the Si substrate is probed as well. While the 17 eV structure (d') increases in intensity, a structure at about 7–8 eV (IPP) develops in the low energy loss region (Figs. 3b and 10, as a result of an enlargement of the low energy loss part).

The two small peaks at 3 eV and 6 eV labelled (1) and (2), which are observed at low primary energy, are progressively shifted to peaks 3.7 and 5.2 eV (referred to as (1′) and (2′), see Table 3).

To understand these evolutions, we have used as a second step the model developed in Section 3.2 for a substrate/overlayer interface. The parameters of the Si dielectric function were fitted from the optical data [37] (Table 6). The experimental single scattering cross-section at the highest primary energy ($E_p = 1543$ eV) was fitted using Eq. (5) with the parameters of the dielectric function ($\hbar\omega_j, f_j, \gamma_{j\,\mathrm{optical}}$) for Si and SiO_2 fitted from the optical data (Tables 4 and 6; Fig. 11a). To limit the number of fitting parameters, the d_1–d_4 thicknesses were kept constant ($d_1 = 0.75$ nm, $d_2 = 1.65$ nm, $d_3 = 2.05$ nm, $d_4 = 2.45$ nm) and only the two free parameters A_{Si}, A_{SiO_2} were allowed to vary. Then in a second step, only the γ_j parameters were allowed to vary (Fig. 11b), and the best fit of the parameters for Si ($\gamma_{j\,\mathrm{REELS}}$) is given in Table 6. The peak at 34 eV cannot be reproduced because it is due to multiple scattering. As expected, the silicon bulk plasmon (d') at 17 eV (Fig. 11b) is well described by the bulk silicon ELF ($\mathrm{Im}[-1/(\varepsilon^{Si}(\omega))]$). The peak around 7–8 eV (IPP) appears to originate only from

Table 6
Drude–Lorentz coefficients for the dielectric function of Si (Eq. (4))

j	$\hbar\omega_j$ (eV)	f_j (eV^2)	$\hbar\gamma_j$ (eV)	
			Optical	REELS
0	17.4	0.005	0.87	0.67
1	4.19	0.417	0.72	1E−7
2	6.71	0.473	3.87	9.81
3	3.49	0.104	0.33	0.008

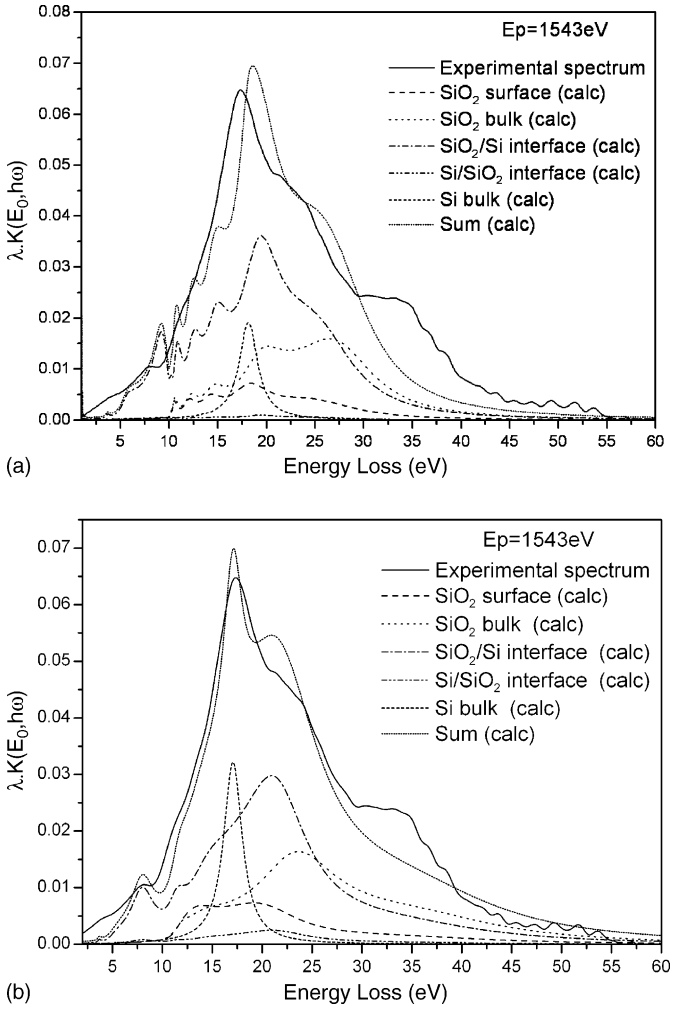

Fig. 11. Decomposition of the experimental single scattering cross-section at $E_p = 1423$ eV into bulk SiO_2, surface SiO_2, interface Si/SiO_2, and bulk Si contributions. The interface contribution is twofold, see Eq. (5) (coefficients C and D). The parameters of the dielectric function for Si and SiO_2 are: (a) the ($\omega_j, f_j, \gamma_{j\,\mathrm{optical}}$) values; (b) the ($\omega_j, f_j, \gamma_{j\,\mathrm{REELS}}$) values from Tables 4 and 6.

the interface ELF ($\mathrm{Im}[-2/(\varepsilon^{SiO_2}(\omega) + \varepsilon^{Si}(\omega))]$). Moreover, this contribution comes mainly from the SiO_2/Si interface within the [d_2–d_3] thicknesses (Fig. 5) because $C(\lambda^{SiO_2}(E_p), \varphi, \phi, Z)$ is larger than $D(\lambda^{Si}(E_p), \varphi, \phi, Z)$, C and D being decreasing functions with the thickness d and increasing functions with the IMFP λ. With the same set of parameters for the dielectric constant (Tables 4 and 6) all the experimental single scattering cross-sections of Fig. 3b were fitted in the same way and the A_{Si}, A_{SiO_2} parameters determined (Table 7).

The simulated scattering cross-sections from $E_p = 418$ to 1543 eV are depicted in Fig. 12. We show in Fig. 13 the fitted bulk and surface contributions, together with the interface contribution of the single scattering cross-section at $E_p = 418$ eV, which had been previously fitted with the simple model of Section 3.1 (Fig. 9d), under the assumption that only the SiO_2 layer was probed. In fact, due to the values of the d_1–d_4 thicknesses used, the consideration of a small contribution of the Si/SiO_2 interface slightly improved the agreement with experiment.

Table 7
A^{SiO_2} and A^{Si} coefficients obtained when decomposing the experimental REELS scattering cross-sections of the SiO_2/Si sample at different E_p into bulk, surface and interface contributions according to Eqs. (5)–(10), by using the $\gamma_{j\,REELS}$ values from Tables 4 and 6

Energy (eV)	A^{SiO_2}	A^{Si}
418	0.00922	1.37×10^{-6}
490	0.00808	0.00094
538	0.0076	0.0011
698	0.0058	0.00076
876	0.00587	0.000761
1024	0.0038	0.00134
1265	0.00294	0.00131
1543	0.00243	0.00127

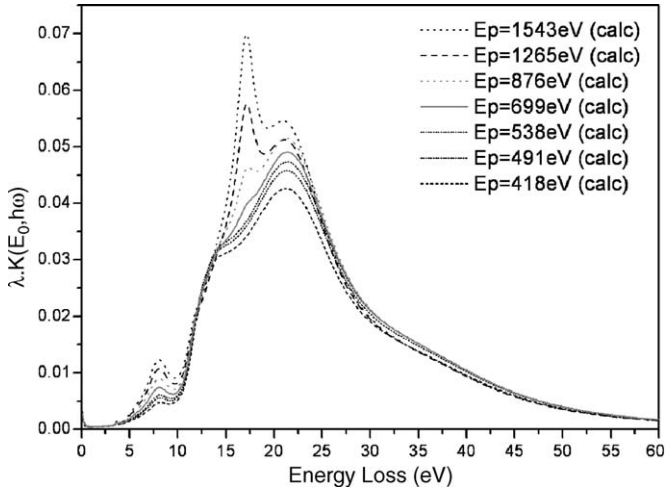

Fig. 12. Comparison of the fitted single scattering cross-sections at different primary energies ranging from $E_p = 418$ to 1543 eV.

The shape of the interface loss function contribution to the scattering cross-section is in fair agreement with the experimental interface loss function obtained by TEELS when measuring the low energy loss spectrum on the SiO_2 side of a Si/SiO_2 interface [25,26], thus validating our model in the present case.

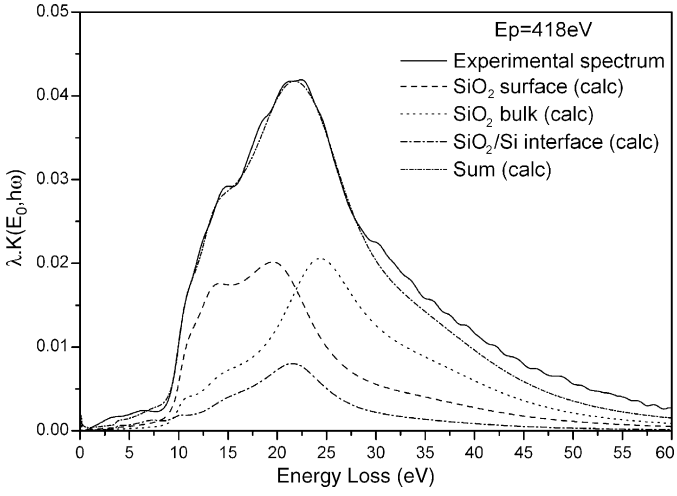

Fig. 13. Decomposition of the experimental scattering cross-sections at $E_p = 418$ eV into bulk, surface and interface contributions following Eq. (5) using the (ω_j,f_j,$\gamma_{j\,REELS}$) parameters from Tables 4 and 6.

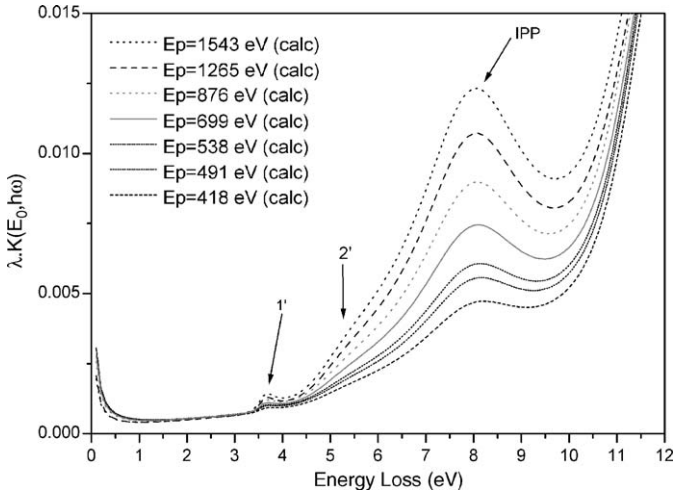

Fig. 14. Enlargement of the low loss energy part of Fig. 12.

The peak around 7–8 eV is due to the excitation of an interface plasmon peak (IPP) already observed by TEELS for silicon covered by a SiO_2 layer. The surface plasmon peak is at 12.2 eV for a clean silicon surface (Si/vacuum interface) and shifts to 7–8 eV when Si is covered by a SiO_2 layer (Si/SiO_2 interface) [26,42]. The shift of the Si surface plasmon peak was also observed by REELS as a function of oxygen exposure of a clean silicon surface [17,43].

Besides this IPP peak, the interface loss function proved to reproduce also the two peaks around 3.5 and 5.3 eV (1′) and (2′), which were observed in the experimental single scattering cross-sections (Fig. 10), and which show up in Fig. 14, where the low energy loss part of the simulated scattering cross-section of Fig. 12 is displayed. These peaks are due to interband transitions in silicon which were already present in the silicon bulk energy loss function [37]. Their intensities are strengthened by the interface loss function.

Contrary to our study with $SrTiO_3$, the presence of a carbon monolayer did not affect our interpretation. The carbon plasmon peak has an energy very close to that of the bulk SiO_2 plasmon peak (e). Spurious effects are expected to be more critical at the lowest primary energies. However, the intensity of the SiO_2 bulk plasmon peak increases with primary energy, as expected from a larger contribution of bulk SiO_2, while the contribution of the carbon plasmon peak is expected to decrease when the primary energy increases. The observed trend is therefore unambiguously related to an increased contribution of the bulk SiO_2 contribution. Moreover, all what concerns the IPP peak should not be affected by the carbon contamination. This makes us confident that REELS can be safely used to studying interfaces in technological samples.

5. Conclusion

We have used a simple model to describe the evolution of the shapes of the REELS single scattering cross-sections as a

function of primary energy. The REELS single scattering cross-sections were written as linear combinations of bulk, surface, and interface electron energy loss functions, where the dielectric function was fitted to optical or valence band-TEELS data.

In the case of our study of the $SrTiO_3$ single crystal, the simulations reproduced the overall observed trends, but the excitation of a plasmon in the thin carbon contamination layer, enhanced at the lowest primary energies, competed with the increase of the surface contribution. A better agreement between experiment and simulations could be likely reached by modelling a $SrTiO_3$/carbon interface instead of a single $SrTiO_3$/vacuum interface, so as to remove the carbon layer contribution.

In the case of the silicon substrate covered by a SiO_2 nanometric layer, our model successfully described the evolution of the shape of the REELS single scattering inelastic cross-sections. In particular, the introduction of the Si/SiO_2 interface electron energy loss function proved necessary to account for the 7–8 eV structure, interpreted as an interface plasmon peak, originating mainly from the SiO_2 side of the interface. The extracted REELS interface loss function compared very well with the previously published TEELS interface loss function at a Si/SiO_2 interface [25,26]. The present work shows that REELS is well suited to studying dielectric properties of interfaces between a substrate and a nanometric layer.

Acknowledgements

This work was supported by the European Union under contract G5D-CT-2001-00586, and by the US NSF award under contract DMR-0010062.

References

[1] F. Yubero, J.M. Sanz, B. Ramskov, S. Tougaard, Phys. Rev. B 53 (1996) 9719;
F. Yubero, D. Fujita, B. Ramskov, S. Tougaard, Phys. Rev. B 53 (1996) 9728.
[2] W.S.M. Werner, Surf. Interface Anal. 35 (2003) 347.
[3] Z.J. Ding, R. Shimizu, Phys. Rev. B 61 (2000) 14128.
[4] C.J. Tung, Y.F. Chen, C.M. Kwei, T.L. Chou, Phys. Rev. B 49 (1994) 16684.
[5] Y.F. Chen, Y.T. Chen, Phys. Rev. B 53 (1996) 4980.
[6] F. Yubero, V.M. Jimenez, A.R. Gonzalez-Elipe, Surf. Sci. 400 (1998) 116.
[7] C.G. Fuentes, E. Elizalde, F. Yubero, J.M. Sanz, Surf. Interface Anal. 33 (2002) 230.
[8] F. Barreca, A.M. Mezzasalma, G. Mondio, F. Neri, S. Trusso, C. Vasi, Thin Solid Films 377–378 (2000) 631.
[9] R. Reiche, F. Yubero, J.P. Espinos, A.R. Gonzalez-Elipe, Surf. Sci. 457 (2000) 199.
[10] W.S.M. Werner, Surf. Sci. 526 (2003) L159.
[11] P. Prieto, S. Hofmann, E. Elizalde, J.M. Sanz, Surf. Interface Anal. 36 (2004) 1392.
[12] P. Prieto, C. Quiros, E. Elizalde, J.M. Sanz, Surf. Interface Anal. 36 (2004) 820.
[13] S. Tougaard, F. Yubero, Surf. Interface Anal. 36 (2004) 824.
[14] S. Tougaard, Surf. Sci. 464 (2000) 233.
[15] T. Nagatomi, Y. Takai, B.V. Crist, K. Goto, R. Shimizu, Surf. Interface Anal. 35 (2003) 174.
[16] Z. Zengming, T. Koshikawa, T. Iyasu, R. Shimizu, K. Goto, Surf. Interface Anal. 35 (2003) 403.
[17] T. Nagatomi, T. Kawano, R. Shimizu, J. Appl. Phys. 83 (1998) 8016.
[18] F. Yubero, S. Tougaard, Phys. Rev. B 46 (1992) 2486.
[19] F. Yubero, J.M. Sanz, J.F. Trigo, E. Elizalde, S. Tougaard, Surf. Interface Anal. 22 (1994) 124.
[20] R.F. Egerton, Electron Energy-Loss Spectroscopy in the Electron Microscope, Second edition, Plenum, New York, 1986.
[21] R.H. Ritchie, Phys. Rev. 106 (1957) 874.
[22] S. Tanuma, C.J. Powell, D.R. Penn, Surf. Interface Anal. 17 (1991) 911.
[23] K. Van Beethem, R.H. French, W. Sigle, C. Elsässer, M. Rühle, Ultramicroscopy 86 (2001) 303.
[24] K. Van Beethem, C. Elsässer, R.H. French, J. Appl. Phys. 90 (2001) 6156.
[25] P. Moreau, N. Brun, C.A. Walsh, C. Colliex, A. Howie, Phys. Rev. B 56 (1997) 6774.
[26] M.A. Turowski, T.F. Kelly, P.E. Batson, J. Appl. Phys. 76 (1994) 3776.
[27] S. Tougaard, I. Chorkendorff, Phys. Rev. B 35 (1987) 6570.
[28] E. Colavita, M. De Crescenzi, L. Papagno, R. Scarmozzino, L.S. Caputi, R. Rosei, E. Tosatti, Phys. Rev. B 25 (1982) 2490.
[29] G. Chiarello, E. Colavita, M. De Crescenzi, S. Nannarone, Phys. Rev. B 29 (1984) 4878.
[30] F. Barreca, A.M. Mezzasalma, G. Mondio, F. Fortunato, S. Trusso, C. Vasi, Phys. Rev. B 62 (2000) 16893.
[31] A.A. Aliev, M.K. Ruzibaeva, A.E. Kim, Vacuum 57 (2000) 243.
[32] F. Yubero, S. Tougaard, E. Elizalde, J.M. Sanz, Surf. Interface Anal. 20 (1993) 719.
[33] QUASES-XS-REELS software package, www.quases.com.
[34] A. Frye, R.H. French, D.A. Bonnell, Z. Metallkd. 94 (2003) 3.
[35] V.E. Henrich, P.A. Cox, The Surface Science of Metal Oxides, Cambridge University Press, 1994, p. 202.
[36] C.J. Powell, Phys. Rev. 175 (1968) 972.
[37] E.D. Palik, Handbook of Optical Constants of solids, Academic, Orlando, FL, 1985.
[38] H. Raether, Excitation of Plasmons and Interband Transitions by Electrons, Springer, Berlin, 1980.
[39] S. Shamm, G. Zanchi, Ultramicroscopy 88 (2001) 211.
[40] S. Kohiki, M. Arai, H. Yoshikawa, S. Fukushima, M. Oku, Y. Waseda, Phys. Rev. B 62 (2000) 7964.
[41] F. Bart, M. Gautier, J.P. Duraud, M. Henriot, Surf. Sci. 274 (1992) 317; M. Gautier-Soyer, in: R.A.B. Devine, J.P. Duraud, E. Dooryhée (Eds.), Structure and Imperfections in Amorphous and Crystalline Silicon Dioxide, John Wiley & Sons Ltd., 2000.
[42] T. Ichinokawa, N. Yawagami, H. Anpo, A. Tamura, Phys. Rev. B 28 (1983) 6151.
[43] H. Ibach, J.E. Rowe, Phys. Rev. B 10 (1974) 710.